Journal of Rock Mechanics and Geotechnical Engineering 18 (2026) 3512–3525

Contents lists available at ScienceDirect

Journal of Rock Mechanics and Geotechnical Engineering

journal homepage: www.jrmge.cn

Full Length Article

Mechanical and microstructural properties of Gonghe granite for enhanced geothermal systems: Thermal effects and energy evolution

Zhouqian Wu [a,b,c], Dongming Zhang [a], Yajin Liang [b,c], Shifeng He [b,c], Heping Xie [b,c], Minghui Li [b,c,*]

[a] State Key Laboratory of Coal Mine Disaster Dynamics and Control, Chongqing University, Chongqing, 400044, China
[b] State Key Laboratory of Intelligent Construction and Healthy Operation and Maintenance of Deep Underground Engineering, College of Civil and Transportation Engineering, Shenzhen University, Shenzhen, 518060, China
[c] Guangdong Provincial Key Laboratory of Deep Earth Sciences and Geothermal Energy Exploitation and Utilization, Institute of Deep Earth Sciences and Green Energy, Shenzhen University, Shenzhen, 518060, China

ARTICLE INFO

Article history:
Received 29 March 2025
Received in revised form
22 May 2025
Accepted 29 June 2025
Available online 29 July 2025

Keywords:
Hot dry rock
Macro-micro mechanical properties
Energy evolution
Fracture toughness
Initiation pressure calculation

ABSTRACT

Investigating the mechanical behavior and microstructural evolution of granite under high temperatures is crucial for optimizing fracturing strategies and ensuring reservoir sustainability in enhanced geothermal systems (EGS) at the Qiabuqia geothermal field, China. This study conducted triaxial compression tests on granite from the Qinghai Gonghe Basin under temperature from 25 °C to 300 °C, examining the effects of temperature and confining pressure on the mechanical properties and energy evolution of the granite. Additionally, X-ray diffraction (XRD) analysis and nanoindentation tests were employed to assess changes in micro-mechanical properties and mineral compositions. Furthermore, fracture mechanics principles, incorporating thermal stress effects, were utilized to calculate the initiation pressure of reservoirs at an engineering scale for geothermal development in the Qinghai Gonghe Basin. The results indicate that the compressive strength and elastic modulus of Gonghe granite increase with temperature up to 200 °C due to the enhancement of mineral mechanical properties and thermal densification, but significantly decrease at 300 °C due to thermal damage and fracture propagation. Energy analysis reveals that the granite undergoes a transition from brittle to ductile behavior under high-temperature conditions. The proportion of energy dissipation during deformation increases with temperature. The increased proportion of quartz, coupled with its high thermal expansion coefficient and elastic modulus, generates intense thermal stress at the interfaces between quartz and adjacent minerals. The development and propagation of transgranular fractures around quartz are critical factors influencing the macroscopic mechanical properties of granite. This study provides a good understanding of the effects of high temperature on granite performance and its engineering significance in reservoir development, emphasizing the role of thermal stress in reducing fracturing pressure and promoting fracture propagation.

1. Introduction

Geothermal energy, a clean and renewable energy source, has garnered widespread global attention (Breede et al., 2013; Pan et al., 2019). Hot dry rock (HDR), a form of geothermal energy, is considered a major direction for future energy development due to its high energy storage potential and environmental friendliness. In recent years, the Qinghai Gonghe Basin in China, with its unique geological characteristics and abundant thermal reservoir resources, has become a focal area for HDR research and development. Among these, the Qiabuqia geothermal field stands out as a representative site, characterized by a high geothermal gradient and thermal flux values, harboring high-quality HDR resources

* Corresponding author. State Key Laboratory of Intelligent Construction and Healthy Operation and Maintenance of Deep Underground Engineering, College of Civil and Transportation Engineering, Shenzhen University, Shenzhen, 518060, China.
E-mail address: mhli@szu.edu.cn (M. Li).

Peer review under responsibility of Institute of Rock and Soil Mechanics, Chinese Academy of Sciences.

https://doi.org/10.1016/j.jrmge.2025.06.016

(Hou et al., 2024). This distinctive geological setting provides a solid foundation for geothermal energy development in China while posing greater challenges for understanding the mechanical behavior of reservoir rocks and the propagation of thermally induced fractures. Therefore, an investigation of the macroscopic mechanical properties and microstructural evolution of HDR reservoir rocks in the Qinghai Gonghe Basin under high-temperature conditions, as well as an exploration of thermal stress and its influence on internal fracture propagation, is critical for understanding and optimizing fracturing and extraction strategies for high-temperature HDR.

Extensive research has focused on the mechanical properties of granite under different temperature treatments, including uniaxial compressive strength (Chen et al., 2012), triaxial compressive strength (Yin et al., 2022), elastic modulus (Sha et al., 2020), and fracture toughness (Chu et al., 2024). In addition to conventional static testing methodologies, Dang et al. (2022) developed a multifunctional dynamic shear apparatus, providing technical support for investigating the behavior of deep-seated rocks under coupled shear-flow and dynamic disturbance. Moreover, machine learning methods have been used to predict the mechanical characteristics of rocks (Le et al., 2022; Asteris et al., 2024). However, these studies have yielded different conclusions. Wu et al. (2019a, b) observed that elevated temperatures lead to degradation of the mechanical parameters, with the degree of degradation becoming more pronounced at higher temperatures. Other researchers found that the mechanical properties of granite generally do not degrade until it is heated to 200–400 °C, and may even increase (Yang et al., 2017; Qin et al., 2020; Hu et al., 2023). However, at higher temperatures, these properties begin to decline, with granite's brittleness first increasing and then decreasing. The threshold temperatures identified in these studies vary significantly. The lithological differences in granite from various regions limit the applicability of these research findings to a specific geothermal reservoir. For instance, in the Qinghai Gonghe Basin, the HDR in the Qiabuqia geothermal field has a unique geological setting. Due to prolonged exposure to deep magmatic heat conduction and tectonic stress, the granite reservoir in this region is different from granite in other regions. To meet the practical demands of HDR development in the Qinghai Gonghe Basin, it is imperative to conduct systematic research on the mechanical properties of granite from this region under high-temperature conditions.

Characterizing the effects of heat on the minerals of granite at the microscale is crucial for better understanding its corresponding macroscopic mechanical behavior. As granite is a complex and heterogeneous composite material, its macroscopic mechanical behavior is determined by its constituent minerals (Vázquez et al., 2015). Many researchers have employed nanoindentation tests to investigate the micro-mechanical behavior of granite. Liu et al. (2023) used nanoindentation techniques to explore the micro-mechanical properties of granite minerals and their interfaces, and suggested that the Young's modulus and hardness of quartz, potassium feldspar, and plagioclase decrease with increasing peak loads. Xie et al. (2024a) analyzed the fracture toughness of granite containing natural fractures using an energy-based method with nanoindentation. Moreover, some researchers have examined the relationship between mineral mechanical properties and temperature. Maruvanchery and Kim (2020) investigated the reduced modulus and hardness of major minerals within rocks, such as quartz, calcite, plagioclase, and potassium feldspar, under high temperatures. Mo et al. (2022) studied the micro-mechanical properties of minerals in Gonghe granite during heating-cooling cycles and concluded that the reduced modulus and hardness of quartz, the primary constituent mineral, decrease during the heating process and subsequently increase during the cooling phase. However, existing studies have predominantly focused on the degradation behavior of mechanical parameters at either the macroscopic or the microscopic scale in isolation, and the interrelationship among macroscopic mechanical response, the evolution of microscopic physico-mechanical properties, and energy-dissipation mechanisms remains inadequately explored. Throughout the entire rock-failure process, the patterns of energy input and dissipation directly reflect the evolution of internal damage and the mechanisms governing the brittle-to-ductile transition. Moreover, in Enhanced Geothermal System (EGS) operations, thermally induced stresses arising from temperature differentials can markedly reduce the fracture toughness of rock, thereby lowering the breakdown pressure. Current theoretical models for predicting reservoir breakdown pressure fail to adequately quantify thermal stress.

Therefore, this study investigates granite from the Gonghe Basin, Qinghai Province, China, through a series of triaxial compression tests performed at elevated temperatures (25–300 °C) and varying confining pressures. These tests were complemented by X-ray diffraction (XRD) mineralogical analyses, nanoindentation measurements, and scanning electron microscopy (SEM) microstructural observations to systematically elucidate the influence of temperature on the granite's macroscopic mechanical behavior, energy evolution pathways, and microstructural thermal damage mechanisms. Finally, integrating the experimental results with fracture mechanics theory, a predictive model for reservoir fracture initiation pressure accounting for thermal stress effects was established.

2. Experimental set-up

2.1. Sample preparation

The granite used in this study was sampled from the Gonghe Basin, Qinghai Province, China (Fig. 1a). The granite in this region primarily belongs to the Indosinian granite of the Gonghe Basin. The Gonghe Basin is the first area in China. In the Qiabuqia geothermal field, heat from deep magmatic bodies is transferred to shallower granite through concealed faults, while the thick Quaternary sedimentary layers above inhibit heat dissipation, resulting in shallow-buried, high-grade HDR resources (Gao et al., 2018). The GR1 HDR exploration borehole has a depth of 3705 m and a bottom-hole temperature of 236 °C, representing the highest temperature HDR resource currently drilled in China. In this study, granite outcrops are sampled near the Gouhou Reservoir, adjacent to the Qiabuqia geothermal field (Fig. 1b). The sampled granite is medium-to-coarse-grained, grayish-white granite, containing pre-existing natural fractures caused by geological tectonic movements and water erosion. The lithological composition and formation age of the samples are consistent with the granite exposed in the GR1 borehole of the Gonghe Basin. The samples were processed into standard cylindrical specimens with dimensions of 50 mm × 100 mm (diameter × height) according to ISRM standards. To minimize the anisotropy of Gonghe granite and reduce the dispersion in experimental results, longitudinal wave velocities were measured, and samples with similar wave velocity results were selected for the experiments. The basic physical properties of Gonghe granite are shown in Table 1.

2.2. Testing procedure

Considering the defined temperature range for HDR and the bottom-hole temperatures of geothermal wells currently drilled in China, the selected treatment temperatures for this experiment

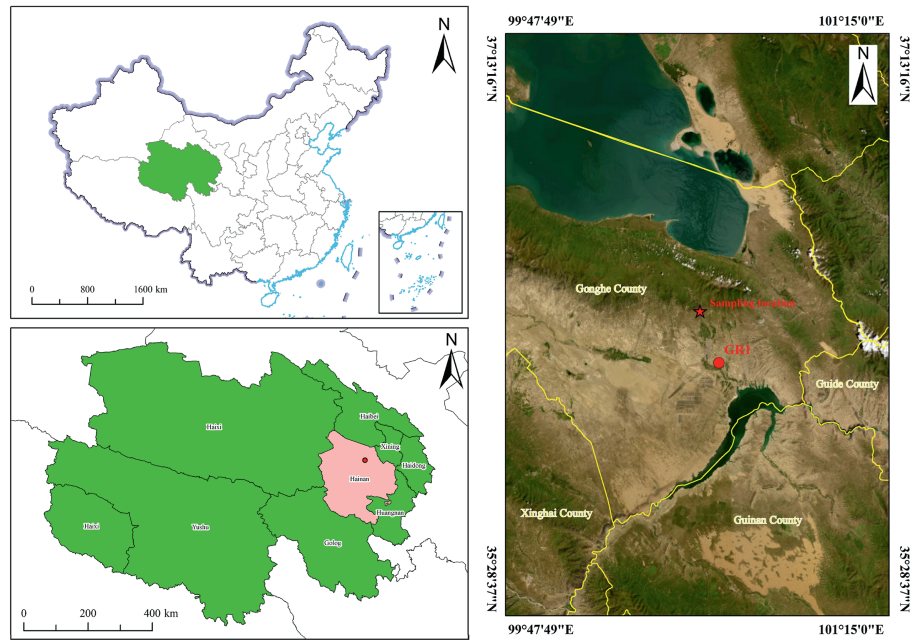

(a)

(b)

Fig. 1. (a) Overview of the Qinghai Gonghe Basin (modified after Lei et al. (2019)), and (b) granite outcrop near the Qiabuqia GR1 geothermal well.

Table 1
The basic physical properties of Gonghe granite.

Density (kg/m^3)	P-wave velocity (m/s)	Porosity (%)	Thermal conductivity (W/(m K))
2679.09	5112.24	0.42	2.66

were 100 °C, 200 °C, and 300 °C, with natural-state granite used as the control group. The heating rate was set at 5 °C/min, and once the target temperature was reached, it was maintained for 6 h, followed by natural cooling to 25 °C under ambient conditions. To characterize the effects of temperature on the mechanical properties of granite and analyze the microscopic mechanisms of thermal damage, a series of experiments are conducted on the granite samples (Fig. 2).

(1) Uniaxial compression and triaxial compression tests were first conducted on granite samples using the GCTS electro-hydraulic servo rock mechanics testing system. At the start of the experiment, confining pressures of 5 MPa, 10 MPa, 20 MPa, 30 MPa, and 40 MPa were applied at a rate of 1 MPa/min.

(2) Axial strain control was then employed at a rate of 0.001 %/min until specimen failure occurred. To characterize the effects of thermal damage at the microscale, XRD test was conducted to reveal the variation in mineral content of the samples with temperature.

(3) Nanoindentation technology was employed to characterize the micromechanical properties of minerals under different temperature conditions. During the testing process, the EDS method was used to identify the mineral composition within the granite, and SEM was applied to observe the morphological characteristics of thermally induced fractures.

(4) Surface images of the granite were captured using the optical microscope integrated with the PI890 indentation instrument, and these images were combined with the EDS

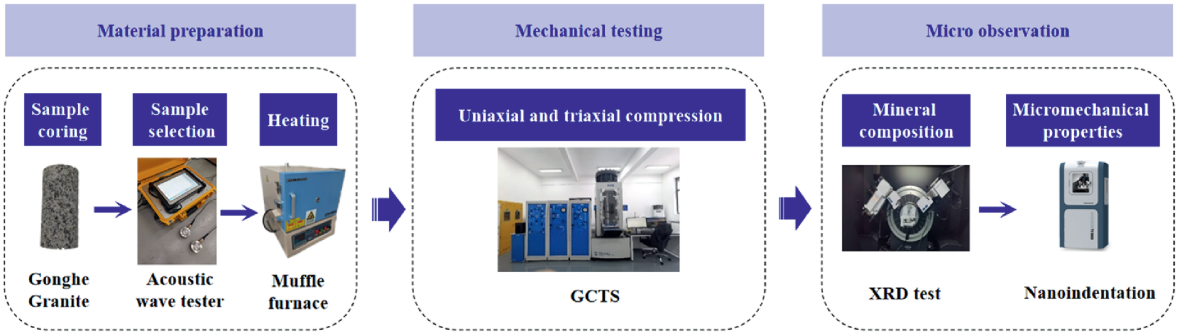

Fig. 2. Experimental testing procedure used in this study.

mapping from the electron microscope to precisely determine the location of the target mineral for indentation.

(5) The probe was brought into contact with the selected mineral, and nanoindentation tests were performed with a loading rate of 10 mN s^{-1}. To enhance the reliability and representativeness of the results, at least three indentation experiments were conducted on each of the four representative minerals in the granite.

3. Results

3.1. Mechanical properties

3.1.1. Stress-strain curve

Fig. 3 illustrates the full stress-strain curves of Gonghe granite under different temperatures and confining pressures. The stress-strain curves can be divided into the compaction stage, elastic stage, stable fracture propagation stage, unstable fracture propagation stage, and post-peak stage. Fig. 3a displays the complete stress-strain curves of Gonghe granite under different temperatures. It reveals that as temperature increases below 200 °C, the curves exhibit upward shifting, indicating that the peak strength of granite gradually increases with rising temperature, accompanied by a slight increase in peak strain. However, when the temperature reaches 300 °C, the curves shift downward and to the right, suggesting a significant increase in peak strain and a clear degradation in peak strength. Moreover, as shown in Fig. 3b–e, with an increase in confining pressure, both the peak strength and axial peak strain increase significantly. The slope of the elastic stage generally increases with higher confining pressure, indicating a gradual increase in elastic modulus; however, the rate of increase diminishes progressively.

In the first stage, as the temperature increases, the nonlinear behavior of the compaction phase decreases before 200 °C. Beyond 200 °C, the compaction phase becomes significantly prolonged. This indicates that the rise in temperature up to 200 °C promotes the gradual closure of initial pores and microfractures within the granite, at 200 °C–300 °C, thermal damage leads to the development and propagation of internal fractures (Fig. 3a). With increasing confining pressure, the nonlinear behavior of the compaction phase progressively weakens. During the elastic stage, as the temperature rises, the linearity of the stress-strain relationship initially strengthens and then deteriorates. This suggests that the ability of granite to resist deformation improves with increasing temperature up to a certain point, but diminishes as thermal damage intensifies at higher temperatures. In the third stage, as the temperature increases, the slope of the axial stress-strain curve slightly increases before 200 °C, and the linearity of the circumferential strain improves, with strength gradually increasing. This indicates a strain-hardening behavior. However, at 200 °C–300 °C, as the temperature rises, internal pores and fractures continue to develop and coalesce, causing the axial stress-strain curve to deviate from linearity, with a reduction in peak strength, exhibiting a clear strain-softening behavior. In Fig. 3b–e, granite exhibits minimal circumferential expansion deformation before reaching the yield point, displaying distinct brittleness. Upon yielding and failure, circumferential strain increases rapidly, demonstrating significant plastic flow. At 300 °C, the length of the yield plateau in the granite is noticeably longer than at other temperatures, indicating that granite at 300 °C transitions gradually from brittle to plastic behavior. Furthermore, as the confining pressure increases, both axial and hoop strains at failure also increase (Fig. 3b–e). High confining pressure suppresses the rapid, unstable propagation of macroscopic fractures, allowing more microcrack development and plastic flow. This manifests as greater pre-peak strain and enhanced post-peak deformability. These observations indicate that increased confining pressure improves the deformability of the granite. By contrast, when temperature rises, the axial and hoop strains at failure remain insensitive, suggesting that under triaxial compression, the deformation of granite is governed primarily by confining pressure rather than by temperature.

3.1.2. Mechanical characteristic parameters

Fig. 4a presents the variation of triaxial compressive strength(σ_p) of granite under different temperatures as a function of confining pressure. At a constant confining pressure, σ_p exhibits a pattern of initially increasing and then decreasing with rising temperature, with 200 °C as the threshold temperature for σ_p. When the treatment temperature is below this temperature, the thermal expansion of minerals induces the closure of internal pores and fractures—a process known as thermal densification—which in turn enhances the overall compactness of the granite. Furthermore, certain minerals undergo lattice adjustments, resulting in a slight increase in mineral hardness, which slightly strengthens the overall strength of the granite. When the treatment temperature exceeds the threshold temperature, due to the anisotropy of granite, the varying thermal expansion coefficients of different minerals cause mismatched thermal deformations, generating thermal stresses that disrupt the bonding forces between minerals. This results in development and propagation of the fractures, which macroscopically manifests as a deterioration of σ_p. Moreover, σ_p subjected to 300 °C heat treatment is lower than that of untreated samples. Additionally, at the same temperature, the difference in σ_p of rock samples treated under varying thermal conditions gradually decreases. Granite strength is primarily influenced by temperature under low confining pressures, while under high confining pressures, it is predominantly governed by the confining pressure.

Fig. 4b illustrates the variation of the elastic modulus (E) of

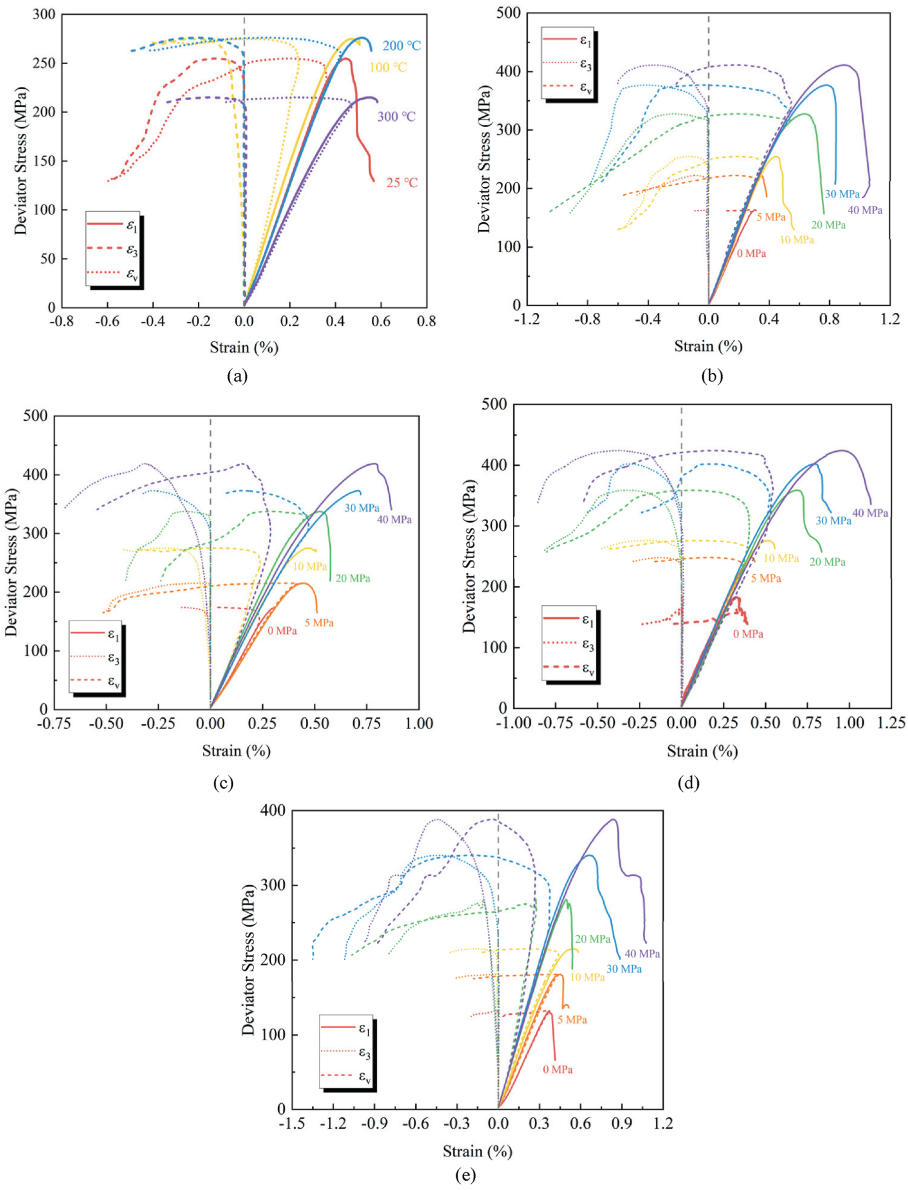

Fig. 3. The complete stress-strain curves of granite after various high-temperature treatments under different confining pressures. (a) 10 MPa confining pressure, (b) natural state, (c) 100 °C, (d) 200 °C, and (e) 300 °C.

granite under different temperatures as a function of confining pressure. It is observed that as the temperature rises from the natural state to 200 °C, E of granite increases slightly. However, when the temperature increases from 200 °C to 300 °C, E decreases rapidly, and this change is more pronounced under low confining pressures. Additionally, as confining pressure increases, E exhibits a nonlinear growth pattern, and the variation in E becomes smaller with increasing confining pressure, indicating that the effect of temperature on E diminishes with higher confining pressures. When the temperature reaches 200 °C, the thermal stresses generated are insufficient to damage the bonding forces between minerals. In fact, they may even enhance the bonding between particles, while the release of free and bound water increases the friction between grains, confirming that the strength of granite improves within this temperature range. At 200 °C–300 °C, thermal fractures gradually initiate and propagate, causing E to decrease sharply.

3.1.3. Stress characteristic strength

Accurately identifying the fracture closure stress (σ_{cc}), fracture initiation stress (σ_{ci}), and fracture damage stress (σ_{cd}) is a prerequisite for geothermal reservoir exploitation. The σ_{cc} marks the end of the initial concave segment in the axial stress-strain curve, which is primarily attributed to the closure of microfractures within the granite. This value is determined using the axial strain response (ASR) method (Peng et al., 2015). The σ_{ci} refers to the critical strength at which fractures within the rock begin to initiate. From this critical point onward, further fracture propagation requires an increase in external load to drive the process, making it the starting point of stable fracture propagation. The σ_{ci} is identified using the lateral strain response (LSR) method (Nicksiar and Martin, 2012). The σ_{cd} represents the point at which many fractures within the rock become interconnected and penetrate through the structure. At this stage, the volumetric strain curve bends, and further fracture propagation and penetration no longer require an increase in external force, signifying

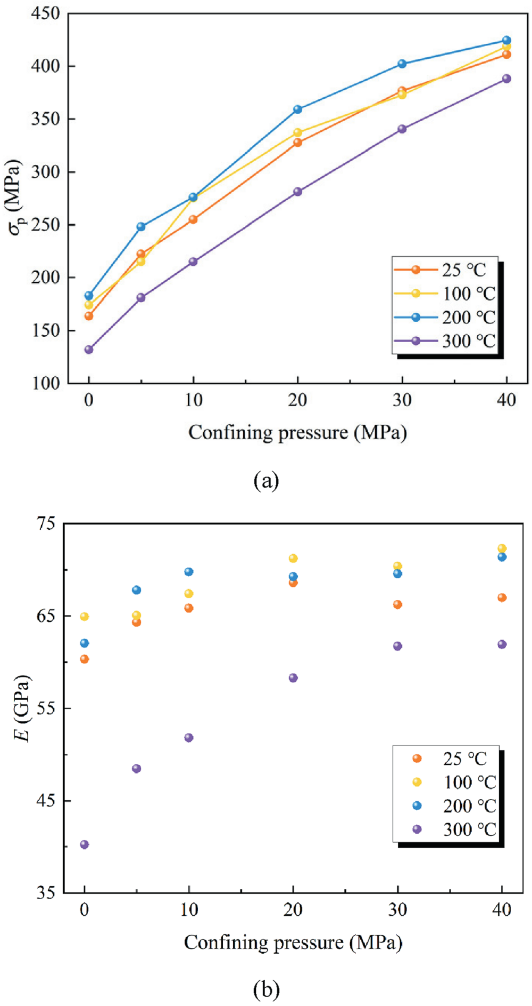

Fig. 4. Variation patterns of mechanical properties of granite under different temperature and confining pressure conditions: (a) Compressive strength, and (b) elastic modulus.

the onset of unstable fracture propagation. The σ_{cd} can be determined from the inflection point of the volumetric strain-axial strain curve (Brace et al., 1966).

Table 2 illustrates the evolution of characteristic stress values with temperature and confining pressure. It can be observed that as the temperature increases, σ_{ci} and σ_{cd} gradually rise before reaching 200 °C, after which they begin to decline rapidly at 300 °C. Furthermore, under higher confining pressures, the temperature effect on σ_{ci} and σ_{cd} is notably diminished compared to lower confining pressures. Additionally, as confining pressure increases, σ_{ci} and σ_{cd} increase, indicating that application of confining pressure facilitates the closure of thermal fractures, thereby enhancing the overall load-bearing capacity of the granite.

Fig. 5a and b illustrates the stress threshold ratios of granite under different temperature treatments. At the same confining pressure, the σ_{ci}/σ_p ratio decreases initially and then increases with rising temperature, whereas the σ_{ci}/σ_p and σ_{cd}/σ_p ratios exhibit no significant change before 200 °C, showing a slight increase, but decrease at 300 °C. Before 200 °C, with rising temperature, the fracture closure region and the region of unstable fracture propagation expand, while the elastic deformation region and the stable fracture propagation region shrink. The degree of fracture development shows varying trends with increasing temperature.

Table 2
Characteristic stress values of granite under different temperatures and confining pressures.

T (°C)	σ_3 (MPa)	σ_{cc} (MPa)	σ_{ci} (MPa)	σ_{cd} (MPa)	σ_p (MPa)	σ_{ci}/σ_p	σ_{cd}/σ_p
25	0	49.269	141.919	159.997	163.817	0.866	0.977
	5	77.667	209.370	212.383	222.397	0.941	0.955
	10	61.167	207.057	233.467	254.897	0.812	0.916
	20	73.622	275.745	316.858	327.514	0.842	0.967
	30	68.068	279.64	331.583	376.732	0.742	0.880
	40	89.048	336.663	348.622	410.913	0.819	0.848
100	0	61.332	124.208	154.246	174.165	0.713	0.886
	5	54.657	207.252	214.529	214.994	0.964	0.998
	10	74.725	141.280	249.545	275.155	0.513	0.907
	20	84.487	306.541	330.638	337.082	0.909	0.981
	30	56.683	287.758	311.713	372.885	0.772	0.836
	40	97.920	217.784	302.885	418.576	0.520	0.724
200	0	51.452	131.046	161.499	182.792	0.717	0.884
	5	53.202	175.417	237.075	248.188	0.707	0.955
	10	66.185	233.595	260.117	276.102	0.846	0.942
	20	67.391	220.905	295.710	359.076	0.615	0.824
	30	62.326	312.721	348.795	402.039	0.778	0.868
	40	83.756	285.277	361.943	424.446	0.672	0.853
300	0	46.449	100.226	116.540	131.905	0.760	0.884
	5	51.716	135.384	176.984	180.875	0.748	0.978
	10	65.174	157.707	206.442	215.031	0.733	0.960
	20	65.905	232.581	267.853	281.118	0.827	0.953
	30	61.476	189.779	268.920	340.430	0.557	0.790
	40	71.786	183.962	312.086	388.093	0.474	0.804

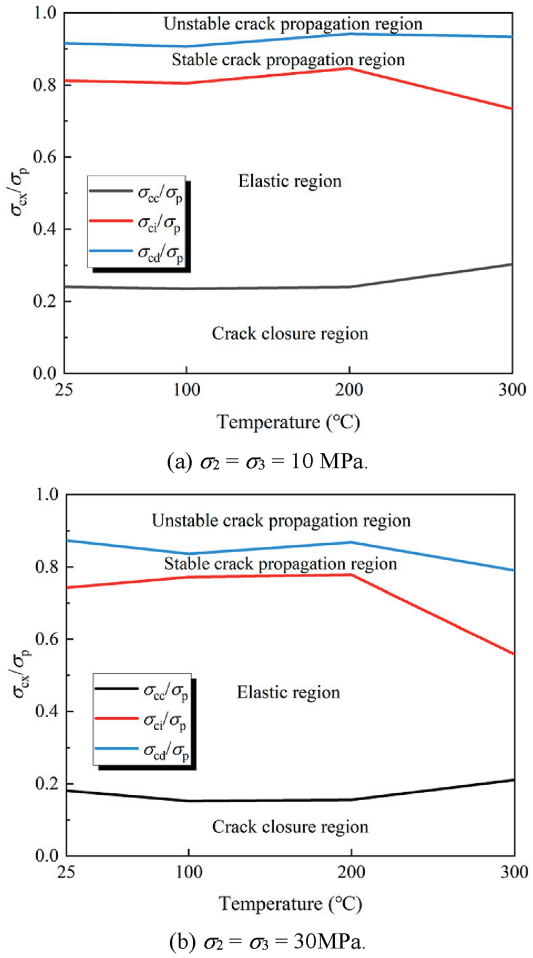

Fig. 5. Stress threshold ratios of granite under different temperature treatments.

The reduction in the fracture closure region indicates that the rise in temperature suppresses the development of pores and fractures, leading to greater overall compactness of the granite. Moreover, the expansion of the elastic deformation region suggests an enhancement in the brittle characteristics of the granite.

The overall proportion of the stable and unstable fracture propagation regions decreases because the thermal stress is insufficient to significantly alter the internal mineral structure of the rock. The thermal expansion of crystals is not enough to induce the thermal fractures and may even lead to the closure of existing pores and fractures. Additionally, the release of free and bound water increases the friction coefficient between grains (Yang et al., 2017), thereby enhancing the overall stiffness of the granite and increasing the difficulty of fracture initiation. When the temperature exceeds 200 °C, the increase in the fracture closure region indicates that granite treated at higher temperatures has undergone more severe thermal damage. Beyond the threshold temperature, as the temperature rises, the elastic deformation region begins to shrink significantly, suggesting that the brittle characteristics of granite weaken and gradually transition to plastic behavior, with the deformation resistance of the matrix significantly reduced. Furthermore, the increase in the stable and unstable fracture propagation regions within this temperature range implies that when the temperature exceeds 200 °C, higher temperatures lead to earlier fracture damage during loading. The degree and rate of fracture damage also increase correspondingly with the rise in temperature (Kumari et al., 2017).

3.1.4. Energy evolution patterns

During the loading process, rocks undergo energy input, storage, dissipation, and release. The loading equipment primarily provides energy input, which is stored in the rock as elastic strain energy and gradually released during plastic deformation and fracture development. As shown in Fig. 6, the energy evolution curve can be divided into three stages:

(1) Compaction stage: The total absorbed energy (U), elastic strain energy (U_e), and dissipated strain energy (U_d) all increase slowly. Most of the external work is converted into U_e and stored within the rock, while the increase in U_d is minimal.
(2) Elastic stage: Both U and U_e increase with deformation, with U_e rising rapidly, while U_d does no increase.

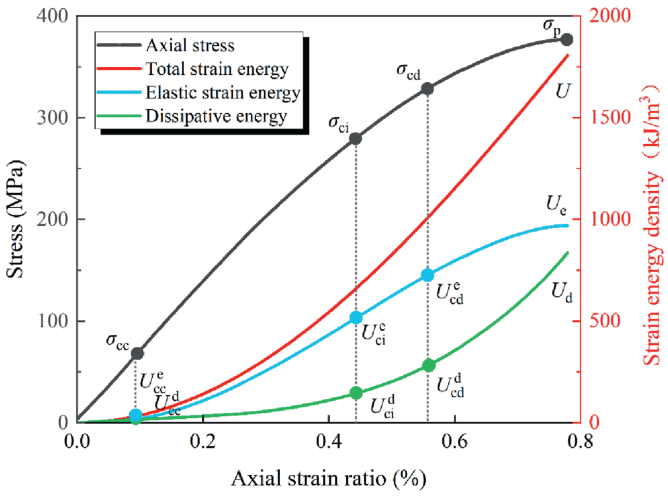

Fig. 6. The relationship between U, U_e and U_d with axial strain.

(3) Fracture propagation Stage: U_d increases sharply, while the growth rate of U_e slows down and reaches its maximum value at the peak strength.

Assuming that the total input strain energy of granite is generated by the work done by the testing machine, and no heat exchange occurs with the external environment during the entire loading deformation process, the system can be regarded as a closed system. According to the first law of thermodynamics, we have

$$U = U_e + U_d \tag{1}$$

where U_e represents the elastic strain energy density (kJ/m^3), and U_d denotes the dissipated energy density (kJ/m^3). Assuming the rock is homogeneous and isotropic during the loading process, the total strain energy that can be accumulated in a rock mass element in the principal stress space is calculated by

$$U = \int_0^{\varepsilon_1} \sigma_1 \mathrm{d}\varepsilon_1 + \int_0^{\varepsilon_2} \sigma_2 \mathrm{d}\varepsilon_2 + \int_0^{\varepsilon_3} \sigma_3 \mathrm{d}\varepsilon_3 \tag{2}$$

where σ_1, σ_2 and σ_3 represent the first, second, and third principal stresses of the rock mass, respectively (in MPa); and ε_1, ε_2 and ε_3 are the principal strains corresponding to the principal stresses of the rock mass element. U_e can be calculated using

$$U_e = \frac{1}{2}\sigma_1\varepsilon_1 + \frac{1}{2}\sigma_2\varepsilon_2 + \frac{1}{2}\sigma_3\varepsilon_3 \tag{3}$$

According to Hooke's law, Eq. (3) can be rewritten as

$$U_e = \frac{1}{2E_0}\left[\sigma_1^2 + \sigma_2^2 + \sigma_3^2 - 2\nu(\sigma_1\sigma_2 + \sigma_1\sigma_3 + \sigma_2\sigma_3)\right] \tag{4}$$

Under uniaxial compression conditions, Eq. (4) can be simplified as

$$U_e = \frac{1}{2E_0}\sigma_1^2 \tag{5}$$

Fig. 7a and b illustrates the variations in total strain energy U, elastic energy U_e, and dissipated energy U_d of granite under different confining pressures as a function of temperature. It can be observed that U for granite gradually increases with temperature before reaching 200 °C. This is attributed to the macroscopic increase in compressive strength with rising temperature, while the peak strain remains relatively unchanged. Microscopically, the thermal expansion effect causes the closure of some pores and fractures, resulting in a denser internal structure of the granite, thereby increasing its strength and stiffness, and allowing it to store more energy. As the temperature continues to rise, at 200 °C–300 °C, thermal shock leads to the further expansion and interconnection of pores and fractures, causing severe thermal damage to the granite's structure. Consequently, the strength decreases significantly, and U shows a marked reduction.

To better contrast the effects of temperature on U_e and U_d, Fig. 7c presents the variation patterns of the elastic strain energy ratio U_e/U and the dissipated strain energy ratio U_d/U. U_e/U is defined as the energy brittleness index B_w (Hucka and Das, 1974), which accounts for the combined influence of stress and strain. It reflects the brittle characteristics of rocks before the peak load. Therefore, B_w is utilized to analyze the brittle-ductile transition behavior of granite after high-temperature treatment. As shown in Fig. 7c, before 200 °C, as the temperature increases, under a confining pressure of 10 MPa, U_e/U rises from 75.46 % to 78.16 %, while U_d/U decreases from 24.54 % to 21.84 %. Within this temperature range, the closure of microfractures occurs inside the

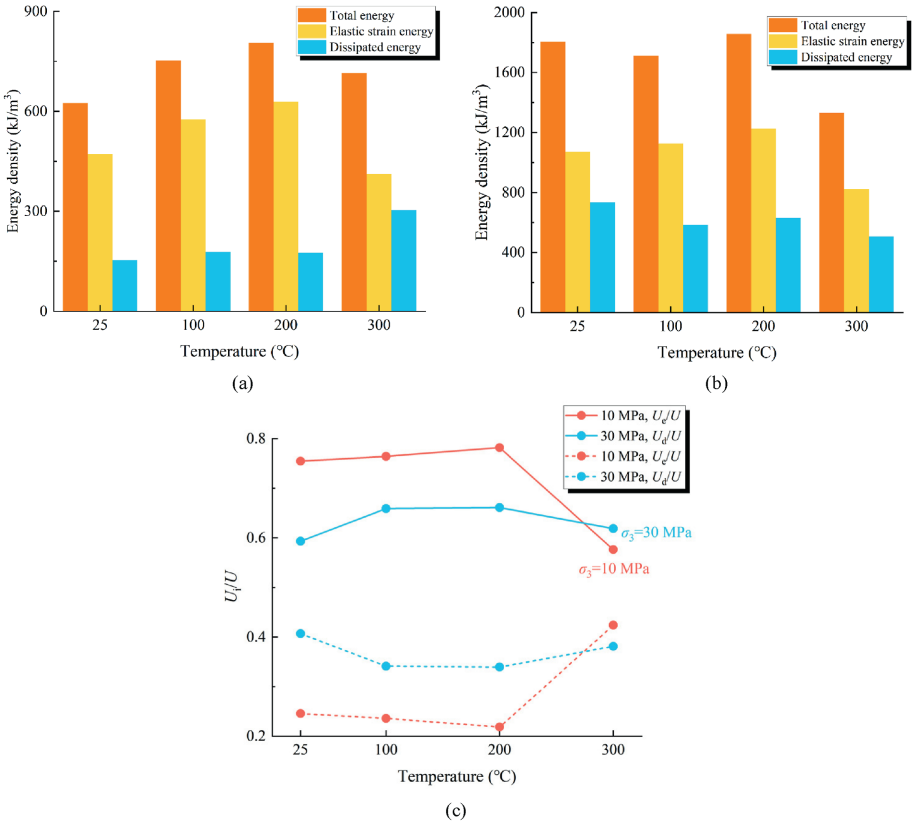

Fig. 7. The variation patterns of U, U_e and U_d of granite with temperature. (a) $\sigma_2 = \sigma_3 = 10$ MPa, (b) $\sigma_2 = \sigma_3 = 30$ MPa, and (c) variation patterns of U_e/U and U_d/U with temperature.

granite, leading to an increase in elastic modulus. As a result, the granite can store more elastic strain energy, making elastic strain energy dominant and enhancing the brittle characteristics of the granite. When the temperature continues to rise to 300 °C, under a confining pressure of 10 MPa, U_e/U decreases from 78.16 % to 57.62 %, while U_d/U increases from 21.84 % to 42.38 %. This is attributed to the initial development of thermal fractures within the granite. It shows that with increasing confining pressure, the proportion of elastic strain energy stored in the granite decreases, while the proportion of dissipated energy increases. This is because the normal stress imparted by the confining pressure on fracture surfaces during loading raises the energy required for fracture propagation, thereby hindering fracture opening and growth both along grain boundaries and through grains. As a result, fracture propagation, damage, and localized plastic deformation become more pronounced, causing fracture growth under high confining pressure to dissipate more energy. The elevation of confining pressure helps suppress the embrittlement effect induced by high temperature, and the granite's behavior gradually transitions from brittle to more ductile. Furthermore, it can be observed from Fig. 7c that as the confining pressure increases, the difference between U_e/U and U_d/U becomes smaller, and their variation diminishes under higher confining pressures. This indicates that higher confining pressures are conducive to storing greater dissipated strain energy, significantly suppressing the brittleness enhancement effect caused by the temperature increase in granite.

The elastic strain energy and dissipated energy corresponding to σ_{cc}, σ_{ci}, and σ_{cd} are denoted as U^e_{cc}, U^e_{ci}, U^e_{cd}, and U^d_{cc}, U^d_{ci}, U^d_{cd}, respectively. Fig. 8 illustrates the relationship between the proportions of each energy characteristic value and temperature. Before 200 °C, as the temperature increases, U^e_{cc}/U_e gradually decreases, while U^e_{ci}/U_e and U^e_{cd}/U_e show the opposite trend. When the temperature rises to 300 °C, U^d_{cc}/U_d increases rapidly, while U^e_{ci}/U_e and U^e_{cd}/U_e begin to decrease. This is consistent with the variation patterns of stress characteristic values shown in Fig. 5a and b. The reason is that before 200 °C, the thermal expansion effect promotes the closure of microfractures, reducing pores and fractures within the granite. This results in a denser structure, an increase in E, and enhanced brittleness. At 300 °C, the internal fractures in the granite gradually become interconnected, and E begins to decrease significantly, leading to a reduction in the proportion of energy storage during the fracture initiation and damage stages. Furthermore, U^d_{cc}/U_d exhibits a trend of first increasing and then decreasing with rising temperature, whereas U^d_{ci}/U_d and U^d_{cd}/U_d show no significant changes before 200 °C. However, at 300 °C, U^d_{ci}/U_d decreases significantly, while U^d_{cd}/U_d increases substantially. This indicates that under high temperatures of 300 °C, the energy consumption for fracture initiation decreases, while the energy consumption during the damage stage increases. This suggests that the proportion of dissipated energy in the plastic stage gradually grows. The reason lies in the fact that when heated to 300 °C, the increased development of internal fracture in granite leads to more severe pre-peak damage during the loading process. Consequently, greater energy is released for fracture development, propagation, and coalescence, resulting in higher dissipated energy.

3.2. Microscopic experimental results

3.2.1. Mineral composition analysis

The mineral composition was identified and quantitatively analyzed through XRD experiments. Granite block samples with dimensions of 3 mm × 3 mm were tested, with the copper anode

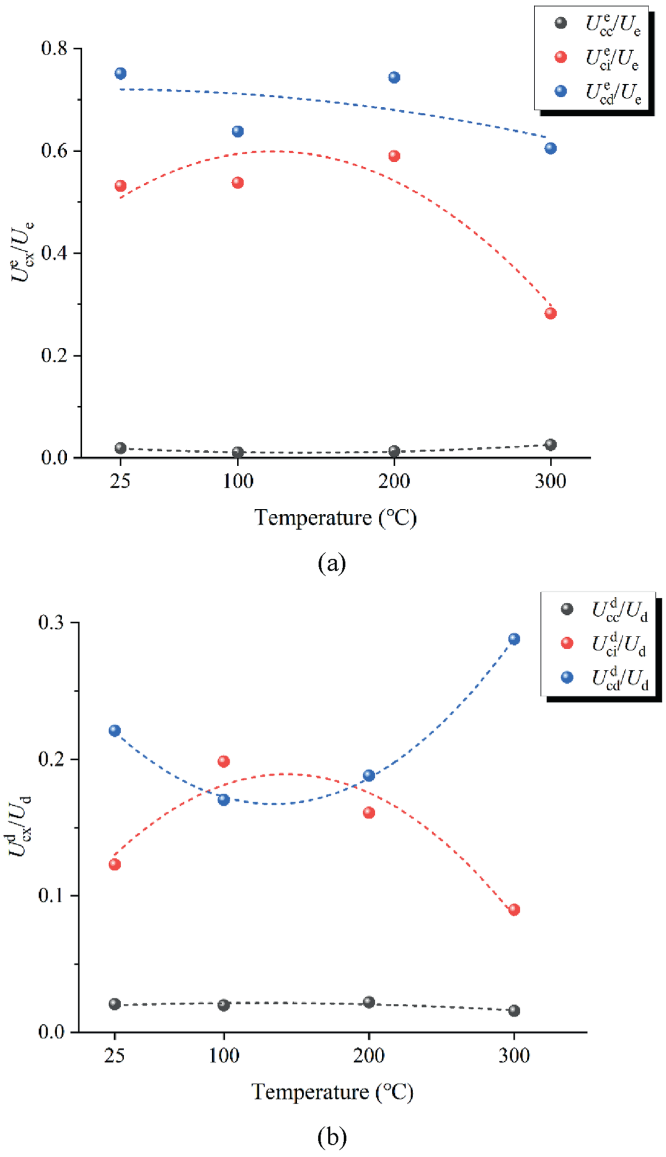

Fig. 8. (a) The variation patterns of U_{cc}^{e}/U_e, U_{ci}^{e}/U_e and U_{cd}^{e}/U_e with temperature, and (b) variation patterns of U_{cc}^{d}/U_d, U_{ci}^{d}/U_d and U_{cd}^{d}/U_d with temperature.

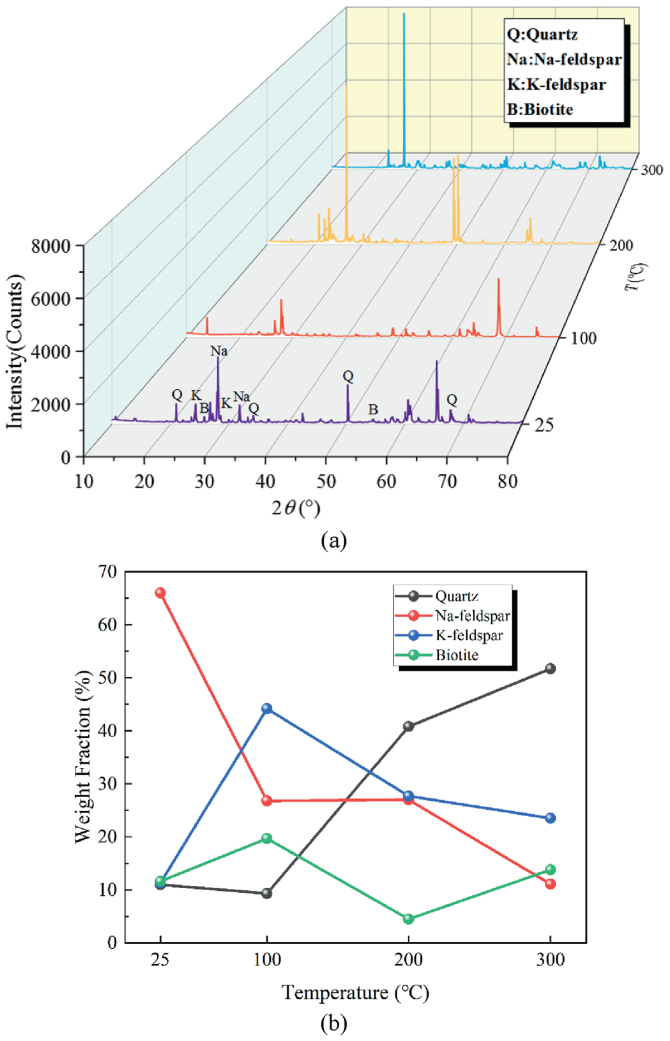

Fig. 9. (a) Granite X-ray diffraction patterns, and (b) variation patterns of mineral content proportions with temperature.

operating at a voltage of 40 kV and a current of 30 mA. Diffraction patterns were recorded over a scanning angle range of $2\theta = 10°$–$80°$, with a scanning speed of 5°/min and an interval of 0.02°/min. The XRD spectra of granite under different temperatures are shown in Fig. 9a. The results indicate that granite is primarily composed of quartz, potassium feldspar, albite, and biotite, accounting for more than 80 % of the total mineral composition. The positions of the diffraction peaks of the main minerals showed no significant shifts or disappearance, suggesting that the primary mineral components did not undergo fundamental changes. However, temperature variations influence the mineral composition's quantitative content.

Fig. 9b compares the mineral composition ratios of granite after thermal treatment at different temperatures. The results show that in its natural state, Na-feldspar has the highest proportion in granite, accounting for 66 %. As the temperature increases, the proportion of Na-feldspar gradually decreases, while the proportion of quartz increases steadily, reaching its highest level of 51.7 % at 300 °C. Additionally, the content of K-feldspar first increases and then decreases, with the threshold temperature of 150 °C. The proportion of biotite exhibits a fluctuating trend, indicating that the increase in temperature has little effect on the biotite content before 300 °C.

3.2.2. Micromechanical properties

The nanoindentation test was employed to explore the evolution of the micromechanical properties of different minerals under the influence of temperature. The mineral composition within granite was primarily identified using the energy dispersive X-ray spectroscopy (EDS) method, with the main mineral components being quartz, biotite, K-feldspar, and Na-feldspar. During the loading and unloading cycles (see Fig. 10), the load-displacement curves are recorded to calculate the Young's modulus E_m and hardness H of the minerals. E_m primarily characterizes the stiffness and elastic deformation capacity of minerals, reflecting the ease or difficulty of deformation under external forces. H represents the resistance of minerals to indentation or plastic deformation. The specific calculation formulas are as follows:

$$h_c = h_{max} - \varepsilon \frac{P_{max}}{S} \tag{6}$$

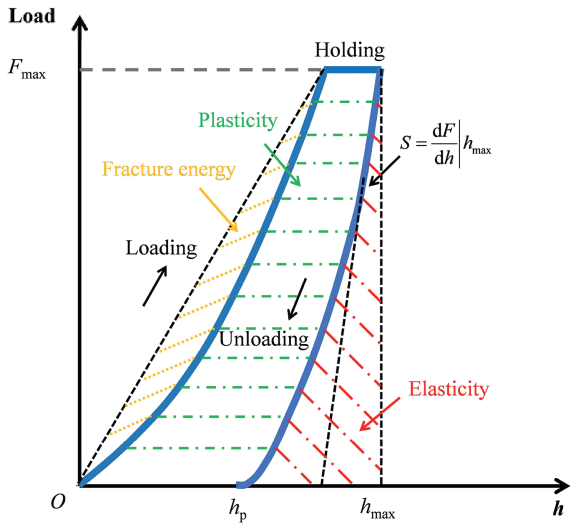

Fig. 10. Typical load-displacement curve.

$$E_r = \frac{\sqrt{\pi}}{2\beta}\frac{S}{\sqrt{A_c}} \tag{7}$$

$$\frac{1}{E_r} = \frac{1-\nu}{E} + \frac{1-\nu_i^2}{E_i} \tag{8}$$

$$H = \frac{P_{max}}{A_c} \tag{9}$$

where P_{max} is the maximum load; and S is the elastic contact stiffness, obtained as the slope of the upper portion of the unloading curve in the elastic stage. E_r is the reduced modulus, representing the combined modulus of the indenter and the test material. E_i and ν_i are the elastic modulus and Poisson's ratio of the diamond indenter, respectively. β is the correction factor for the indenter. ε is a constant related to the shape of the indenter. h_c is the contact depth, and A_c is the projected contact area.

The E_m and H of the four main minerals are shown in Fig. 11. It can be observed that quartz exhibits the highest E_m and H values compared to the other minerals, as quartz has the smallest indentation depth and residual depth. Biotite, on the other hand, is relatively soft, exhibiting significant plastic deformation. When the temperature increases from the natural state to 200 °C, the E_m of quartz increases from 92.22 GPa to 95.20 GPa and then decreases to 90.98 GPa, while H shows a continuous upward trend, increasing by 6.77 % at 200 °C compared to the natural state. This is because the atomic arrangement within quartz becomes more compact, and the lattice tends toward a more stable state. For biotite, E_m and H gradually decrease, dropping by 26.81 % and 22.61 %, respectively, at 200 °C compared to the natural state. For Na-feldspar, E_m and H initially increase and then decrease, following a trend similar to quartz. The E_m and H of K-feldspar, however, both increase steadily, with increases of 3.74 % and 0.64 %, respectively. At 300 °C, except for the increase in E_m of Na-feldspar, the E_m and H of all other minerals begin to decrease. The E_m of quartz, Na-feldspar, and biotite decreases by 2.19 %, 12.13 %, and 23.8 %, respectively, while the H of quartz, Na-feldspar, K-feldspar, and biotite decreases by 4.30 %, 0.84 %, 8.31 %, and 27.40 %, respectively.

As shown in Fig. 11a, before 200 °C, as the temperature increases, the E_m of the primary minerals in granite, such as quartz, K-feldspar, and Na-feldspar, shows varying degrees of

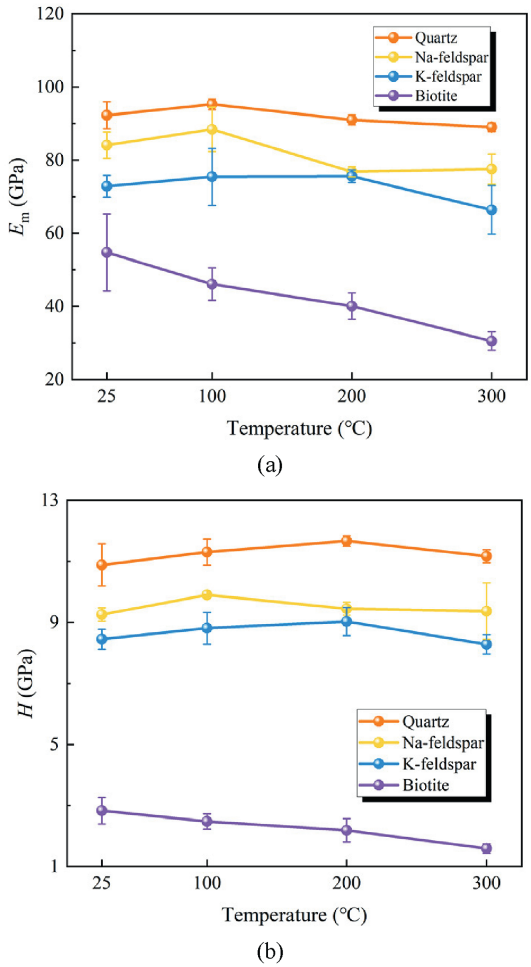

Fig. 11. The variation patterns of E_m and H of different minerals with temperature.

enhancement. This is attributed to the recrystallization of minerals at high temperatures. The growth of potassium feldspar and quartz crystals compresses fractures, and the thermal stress between local mineral particles after high-temperature treatment exceeds the thermal stress caused by thermal expansion. This leads to tighter bonding between mineral particles, enhanced inter-mineral constraints, and increased overall compactness of the granite. Moreover, the H of quartz, K-feldspar, and Na-feldspar also increases with rising temperature (Fig. 11b). This indicates an improved ability of the minerals to resist localized plastic deformation, effectively suppressing plastic flow and microfracture propagation during the compression process. Although the E_m and H of biotite gradually decrease during the heating process, the impact on the overall mechanical properties of granite is not significant due to its relatively low content and its comparatively E_m and H than the other primary minerals. At 300 °C, the E_m and H of quartz and K-feldspar begin to decline. High temperatures weaken the lattice strength and bonding forces of the minerals, leading to a deterioration in their mechanical properties. The reduction in E_m reflects a decrease in the overall stiffness of the granite, while the decrease in H makes fractures easier to form and propagate. Ultimately, this results in a reduction in the macroscopic mechanical parameters of the granite. This observation also highlights that the variation in the micro-mechanical parameters of minerals aligns with the changes in the overall mechanical parameters of granite.

4. Discussion

4.1. The correlation between microscopic fracture toughness and macroscopic mechanical property

Rock fracture toughness is an indicator of its fracturability. The magnitude of fracture toughness reflects the amount of fracture energy required for rock fracturing. Lower fracture toughness facilitates the formation of a more complex fracture network. Fracture toughness K_c can be expressed as

$$K_c = \sqrt{G_c E_r} \tag{10}$$

where G_c is the critical energy release rate, which can be expressed as the ratio of the fracture energy U_c to the contact projected area A_c. U_c and A_c are defined as follows:

$$G_c = \frac{\partial U_{cm}}{\partial A_c} \tag{11}$$

$$U_{cm} = U_m - U_{pm} - U_{em} \tag{12}$$

$$A_c = 24.5 h_c^2 \tag{13}$$

where U_m, U_{cm}, U_{em} and U_{pm} represent the mineral's total energy, fracture energy, elastic energy recovered during the unloading stage, and plastic energy, respectively.

Fig. 10 illustrates the calculation regions for each energy component. Fig. 12 shows the variation of K_c with temperature for the four minerals: quartz, Na-feldspar, K-feldspar, and biotite. The K_c of quartz and K-feldspar exhibits a trend of initially decreasing and then increasing with rising temperature, at a threshold temperature of 200 °C. However, the magnitude of change in K-feldspar is significantly greater than that of quartz. In contrast, the K_c of Na-feldspar exhibits a trend of initially increasing and then decreasing with increasing temperature. Biotite's K_c gradually decreases with rising temperature. The crystal structure of quartz remains relatively stable before its phase transition temperature (573 °C), with no significant phase transformation or reorganization occurring. Its behavior is primarily influenced by the thermal expansion effect. The decrease in K_c of Na-feldspar before 200 °C can be attributed to increased brittleness of the mineral as the temperature increases; whereas at 300 °C, its plasticity increases. The plastic deformation of Na-feldspar decreases initially and then increases, accompanied by variations in indentation depth. Since K_c decreases with increasing indentation depth (Xie et al., 2024b), this explains the observed variation in Na-feldspar's K_c. The K_c of K-feldspar shows a similar trend to the compressive strength of granite, increasing with temperature before 200 °C and then decreasing at 300 °C.

Fig. 11b calculates the correlation coefficients and significance levels between the K_c of the four minerals and the compressive strength of granite. The correlation coefficient and p-value between the K_c of K-feldspar and the strength of granite are 0.985 and 0.015, respectively. This indicates a very strong positive linear correlation between the two, and this correlation is statistically significant. Na-feldspar shows a relatively strong negative linear correlation between its K_c and granite strength, but it has not reached a statistically significant level. The correlation between the K_c of quartz and biotite and the strength of granite is relatively weak. This suggests that the K_c of K-feldspar plays a crucial role in determining the overall matrix strength of granite. As a primary mineral in the granite matrix, the crystal structure and thermal expansion properties of K-feldspar significantly influence the matrix strength of granite. In contrast, the influence of other minerals on the overall strength of granite shows substantial variability.

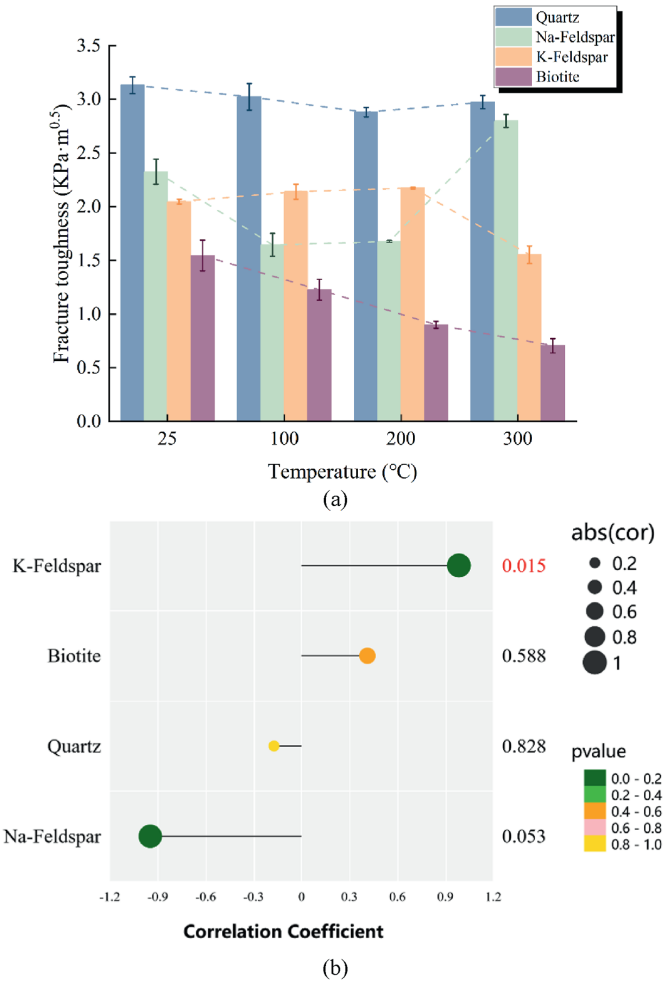

Fig. 12. (a) The variation patterns of K_c for the four minerals at different temperatures, and (b) correlation between K_c and compressive strength.

4.2. The impact of thermal fracture propagation patterns on mechanical properties

The influence of temperature on the macroscopic mechanical properties of granite is primarily governed by the mechanical properties of the matrix minerals and the formation and propagation of thermal fractures. From the SEM results shown in Fig. 12a–c, it can be observed that the microstructure of granite remains largely intact below 200 °C, with some microfractures and pores closing. The increase in temperature improves the mechanical properties of various minerals, thereby enhancing the macroscopic mechanical characteristics of granite and gradually increasing its brittleness. When the temperature rises to 300 °C, thermal shock induces thermal stresses in the rock's internal minerals, which is oriented perpendicular to the grain boundaries. These thermal stresses can be expressed by (Yin et al., 2021):

$$\sigma_{\Delta T} = \frac{(\alpha_1 - \alpha_2)\Delta T E_1 E_2}{E_1 + E_2} = \frac{(\alpha_1 - \alpha_2)\Delta T}{1/E_1 + 1/E_2} \tag{14}$$

where E_1, E_2 and α_1, α_2 are the elastic moduli and thermal expansion coefficients of two adjacent minerals, respectively; and ΔT

represents the temperature difference.

When the thermal stress exceeds the bonding strength at the interface of mineral crystals, thermal fractures begin to form both in between minerals. Eq. (14) indicates that the magnitude of thermal stress is primarily related to the elastic modulus and thermal expansion coefficients of the minerals. As shown in Fig. 13d, transgranular fractures gradually develop and increase within the minerals, especially near quartz. Transgranular fractures are a mode of fracturing in which cracks directly penetrate and traverse mineral crystals. This phenomenon is due to quartz having a higher E_m after thermal treatment compared to other minerals, as well as the significant differences in thermal expansion coefficients among the minerals composing granite. Quartz has a thermal expansion coefficient of approximately 24.3×10^{-6} K^{-1}, whereas feldspar and biotite have values of about 8.7×10^{-6} K^{-1} and 3.0×10^{-6} K^{-1}, respectively (Zhao, 2016). At 300 °C, the lattice of each mineral undergoes thermal expansion, causing stress concentration due to the disparity in thermal expansion coefficients. This stress concentration at the interfaces between different minerals triggers formation of the intergranular fractures. Furthermore, as the temperature rises, the content of quartz increases, resulting in a broader distribution of thermal fractures. The deterioration of granite's crystal mechanical properties leads to development and propagation of the microfractures, which in turn reduces the macroscopic mechanical parameters of granite. This highlights that the formation and expansion of microfractures are the critical factors driving the degradation of granite's macroscopic mechanical properties.

4.3. Calculation of fracture initiation pressure

This section establishes a calculation model for the fracture pressure of HDR reservoirs considering the coupling effect of in situ stress and thermal stress. It also analyzes the variation patterns of reservoir fracture pressure under different depth conditions, combining the geothermal conditions of the Gonghe Basin and the mechanical properties of the Gonghe granite. A method was proposed for calculating formation fracture pressure that considers the influence of three principal stresses in the actual subsurface conditions. For the region surrounding a vertical non-perforated borehole, the hydraulic fracturing initiation pressure P_f is given by

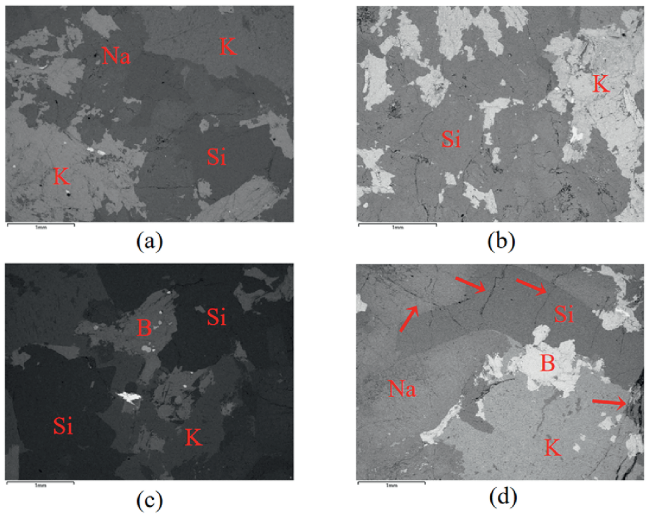

Fig. 13. The internal structural evolution of granite. (a) 25 °C, (b) 100 °C, (c) 200 °C, and (d) 300 °C.

$$P_f = 3\sigma_2 - \sigma_1 - P_p + S_t \tag{15}$$

where σ_1 and σ_2 represent the maximum and minimum horizontal principal stresses, respectively; P_p is the pore pressure of the formation; and S_t is the tensile strength of the reservoir rock. According to field hydraulic fracturing data, the maximum and minimum horizontal principal stresses in the horizontal direction can be expressed as

$$\sigma_1' = \left(\frac{\mu}{1-\mu} + a\right)(S_H - P_p) \tag{16}$$

$$\sigma_2' = \left(\frac{\mu}{1-\mu} + b\right)(S_H - P_p) \tag{17}$$

where a and b are the constants that reflect the magnitude of tectonic stress in the two horizontal principal directions, μ is the Poisson's ratio of the rock formation, and S_H represents the overburden pressure. The overburden pressure can be approximated as the weight of the overlying rock per unit area, calculated by

$$S_H = \gamma H \tag{18}$$

where γ is the unit weight of the overlying rock, and H is the depth from the surface.

During hydraulic fracturing, the high-temperature reservoir of HDR exchanges heat with the cooling medium, causing a temperature reduction in the reservoir. This thermal shock induces thermal stress within the rock, which manifests as tensile stress near the wellbore. This tensile stress significantly affects the initiation and propagation of fractures. Perkins and Gonzalez (1985) calculated the thermal stresses σ_{1T} and σ_{2T} along the directions of the maximum and minimum horizontal principal stresses within an elliptical cooling zone of the reservoir. Assuming the thermal shock zone is circular (Wu et al., 2019a), where the lengths of the major and minor axes are equal, the thermal stresses can be expressed as

$$\sigma_{1T} = \sigma_{2T} = \frac{Ec\Delta T}{2(1-\mu)} \tag{19}$$

where E and c are the elastic modulus and thermal expansion coefficient of the reservoir rock, respectively; and ΔT is the temperature difference. Substituting Eq. (19) into Eq. (15), and applying the effective stress definitions $\sigma_1' = \sigma_1 - P_p$ and $\sigma_2' = \sigma_2 - P_p$, the new formation fracture pressure that considers thermal stress can be derived as

$$P_f = P_p + \left[\frac{2\mu}{1-\mu} - (\alpha - 3\beta)\right](S_H - P_p) - 3\sigma_{1T} + S_t \tag{20}$$

By substituting the macroscopic mechanical parameters of granite obtained in Section 3 into Eq. (20), the initiation pressure of the HDR reservoir under different geothermal temperatures can be calculated. Since there is no fluid medium present in the HDR reservoir, the pore pressure P_p within the rock can be considered 0. Additionally, the vertical principal stress is determined based on geophysical exploration data from the Gonghe Basin in Qinghai. The average geothermal gradient of the Gonghe Basin is 4.73 °C/(100 m) (Zhang et al., 2019a), enabling the calculation of the depth corresponding to the HDR reservoir at different temperatures. The overburden pressure S can then be calculated using Eq. (18), where γ, the unit weight of the overlying rock, is taken as 26.52 kN/m^3. Furthermore, the Poisson's ratio is assumed to be 0.25, the thermal expansion coefficient is taken as 2.5×10^{-6}/°C, and the post-cooling bottom-hole temperature is assumed to be 25 °C. These

parameters can then be used to calculate the initiation pressure of HDR reservoirs under various occurrence depths.

Fig. 14 illustrates the variation in the initiation pressure of Gonghe granite with increasing depth under different reservoir temperatures. It is evident that as the depth of the HDR reservoir increases, the temperature of the reservoir rock also rises, and P_f exhibits a trend of first increasing and then decreasing, with a threshold temperature of 200 °C. Under the influence of the geothermal gradient, the increase in reservoir temperature is typically accompanied by depth increase. With increasing depth, the weight of the overlying rock significantly increases, resulting in a gradual increase in the vertical principal stress and the maximum and minimum horizontal principal stresses. The difference of in situ stresses significantly affects the fracturing process, as a greater principal stress difference requires higher static pressure for fracture propagation. Nanoindentation experimental results indicate that below 200 °C, the E_w and K_c of the main minerals in Gonghe granite, such as quartz, and K-feldspar, increase with temperature, indicating an enhancement in the rock's deformation resistance and significant improvement in its mechanical properties. This necessitates higher initiation pressures during hydraulic fracturing in the reservoir. Above 200 °C, thermal exchange between the bottom-hole cooling medium and the high-temperature reservoir causes significant thermal shock to the reservoir rock, resulting in the propagation and gradual interconnection of microfractures, forming a fracture network. This degrades the overall mechanical properties of the reservoir. Despite the deeper depth and higher in situ stresses of reservoirs at 300 °C, the thermal stress-induced development of pores and fractures becomes dominant, leading to a reduction in P_f.

In the GR1 geothermal well in the Gonghe Basin, the temperature at a depth of 3705 m is 236 °C (Zhang et al., 2019b). This study demonstrates that in the development of EGS, when the temperature of HDR reservoirs exceeds 200 °C, the impact of thermal shock on fracture initiation and propagation is significantly intensified, leading to the degradation of the rock's mechanical properties. Furthermore, the additional thermal stress induced by the injection of low-temperature fluids further reduces the fracture initiation pressure, thereby enhancing the effectiveness of hydraulic fracturing. The findings provide a theoretical basis for the optimization of fracturing strategies in future EGS developments, particularly in high-temperature reservoirs, where thermal stress effects can be leveraged to reduce the complexity of fracturing operations. In practical fracturing engineering for HDR reservoirs, injecting low-temperature fluid media into geothermal

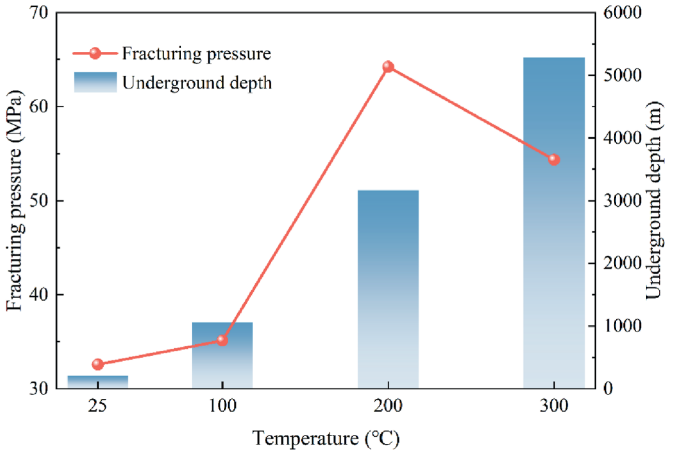

Fig. 14. Variation of fracture initiation pressure in Gonghe HDR at different depths.

reservoirs creates substantial thermal stress due to the temperature differential, which generates and extends fractures within the reservoir rock, thereby forming a connected flow conduit network. In this context, liquid nitrogen fracturing, as an innovative waterless fracturing technique, has been proven to hold great potential for establishing high-permeability pathways. Given that the temperature of liquid nitrogen is −196 °C, the significant temperature difference during thermal exchange with high-temperature reservoirs results in further degradation of the reservoir rock. This process not only improves the connectivity of the internal structure, increasing the permeability of the reservoir rock, but also induces more pronounced mechanical degradation of the rock due to intense thermal fracturing, thus significantly lowering the fracture pressure. Therefore, selecting an appropriate target temperature formation and fracturing fluid, along with precise control over the injection parameters, is crucial for maximizing the effects of thermal stress in enhancing permeability and reducing fracture initiation pressure of HDR reservoir enhancement.

5. Conclusions

This study investigates the macroscopic mechanical properties and microstructural evolution of granite in the Qinghai Gonghe Basin under high-temperature conditions. By employing a combined approach of macroscopic and microscopic analysis, the effects of temperature on the mechanical properties, energy evolution, and thermal damage of granite were explored. The research proposes the correlation between changes in microscopic mineral content and micro-mechanical properties with macroscopic mechanical performance. The main conclusions of the study are as follows:

(1) The macroscopic mechanical parameters of granite, such as compressive strength and elastic modulus, exhibit an increasing trend with rising temperatures up to 200 °C. This is primarily attributed to the thermal expansion effect induced by temperature, which promotes the closure of fractures and results in a denser internal structure of the granite. However, in the temperature range of 200 °C–300 °C, further temperature increases lead to thermal stress, which triggers the initiation and propagation of fractures. This causes a rapid decline in the compressive strength and elastic modulus of granite, with brittle behavior gradually transitioning to ductile behavior.

(2) Below 200 °C, elastic strain energy density dominates, indicating a high degree of brittleness in the granite within this temperature range. At 300 °C, the proportion of dissipated energy increases significantly, reflecting a marked enhancement in the rock's ductility. Energy-based brittleness index analysis shows that granite exhibits enhanced brittleness characteristics below 200 °C. However, at 300 °C, its brittleness decreases notably and the granite gradually transitions to a ductile behavior.

(3) The elastic modulus and hardness of quartz, K-feldspar, and Na-feldspar increase up to 200 °C, but decline between 200 °C and 300 °C due to reduced lattice strength and weakened bonding forces. The mechanical properties of the granite's internal minerals align well with its macroscopic mechanical behavior. Meanwhile, the mechanical parameters of biotite decrease gradually with increasing temperature, but its overall impact on the granite's mechanical performance remains relatively minor. The development of transgranular fractures in quartz minerals is identified as the dominant mechanism driving the formation and

propagation of thermal fractures. The high elastic modulus and thermal expansion coefficient of quartz result in stress concentration within its lattice, while the mismatch in thermal expansion coefficients between different minerals further induces intergranular fracturing, thereby accelerating the degradation of the granite's macroscopic mechanical properties.

(4) Based on the theory of thermal damage, a fracture-pressure model for the reservoir at different depths is established. The results indicate that the fracture initiation pressure of the reservoir increases initially and then decreases with increasing depth. The thermal stress-driven fracture propagation effect reduces the fracture initiation pressure, demonstrating the significant role of thermal stress in enhancing fracturing performance in HDR reservoirs.

CRediT authorship contribution statement

Zhouqian Wu: Investigation, Writing – original draft, Formal analysis. **Dongming Zhang:** Validation, Supervision, Conceptualization. **Yajin Liang:** Data curation, Writing – review & editing. **Shifeng He:** Writing – review & editing, Validation, Investigation. **Heping Xie:** Conceptualization, Methodology, Resources. **Minghui Li:** Resources, Supervision, Funding acquisition, Conceptualization.

Declaration of competing interest

The authors declare that they have no known competing financial interests or personal relationships that could have appeared to influence the work reported in this paper.

Acknowledgments

This work was supported by National key research and development program (Grant No. 2023YFF0723200), National Natural Science Foundation of China (Grant No. 52192625), Shenzhen Science and Technology Program (Grant No. RCYX20221008092903013).

References

Asteris, P.G., Karoglou, M., Skentou, A.D., et al., 2024. Predicting uniaxial compressive strength of rocks using ANN models: incorporating porosity, compressional wave velocity, and schmidt hammer data. Ultrasonics 141, 107347.

Brace, W., Paulding Jr, B., Scholz, C.H., 1966. Dilatancy in the fracture of crystalline rocks. J. Geophys. Res. 71 (16), 3939–3953.

Breede, K., Dzebisashvili, K., Liu, X., Falcone, G., 2013. A systematic review of enhanced (or engineered) geothermal systems: past, present and future. Geotherm. Energy 1, 1–27.

Chen, Y.L., Ni, J., Shao, W., Azzam, R., 2012. Experimental study on the influence of temperature on the mechanical properties of granite under uni-axial compression and fatigue loading. Int. J. Rock Mech. Min. Sci. 56, 62–66.

Chu, P., Xie, H.P., Chen, C.C., et al., 2024. Fracture behavior and fracture surface roughness of high-temperature granite subjected to liquid nitrogen and water cooling. Eng. Fract. Mech. 300, 109987.

Dang, W., Tao, K., Huang, L., et al., 2022. A new multi-function servo control dynamic shear apparatus for geomechanics. Measurement 187, 110345.

Gao, J., Zhang, H.J., Zhang, S.Q., et al., 2018. Three-dimensional magnetotelluric imaging of the geothermal system beneath the Gonghe Basin, Northeast Tibetan Plateau. Geothermics 76, 15–25.

Hou, X.L., Zhong, X.P., Nie, S.S., et al., 2024. Study on the heat recovery behavior of horizontal well systems in the Qiabuqia geothermal area of the Gonghe Basin, China. Energy 286, 129424.

Hu, Y.F., Hu, Y.Q., Jin, P.H., et al., 2023. Real-time mode-I fracture toughness and fracture characteristics of granite from 20 °C to 600 °C. Eng. Fract. Mech. 277, 109001.

Hucka, V., Das, B., 1974. Brittleness determination of rocks by different methods. Int. J. Rock Mech. Min. Sci. 11 (10), 389–392.

Kumari, W.G.P., Ranjith, P.G., Perera, M.B.A., Chen, B.K., Abdulagatov, I.M., 2017. Temperature-dependent mechanical behaviour of Australian strathbogie granite with different cooling treatments. Eng. Geol. Ser. 229, 31–44.

Le, T.T., Skentou, A.D., Mamou, A., et al., 2022. Correlating the unconfined compressive strength of rock with the compressional wave velocity effective porosity and schmidt hammer rebound number using artificial neural networks. Rock Mech. Rock Eng. 55 (11), 6805–6840.

Lei, Z.H., Zhang, Y.J., Yu, Z.W., et al., 2019. Exploratory research into the enhanced geothermal system power generation project: the Qiabuqia geothermal field, Northwest China. Renew. Energy 139, 52–70.

Liu, X., Xu, D., Li, S., et al., 2023. An insight into the mechanical and fracture characterization of minerals and mineral interfaces in granite using nanoindentation and micro X-ray computed tomography. Rock Mech. Rock Eng. 56 (5), 3359–3375.

Maruvanchery, V., Kim, E., 2020. Mechanical characterization of thermally treated calcite-cemented sandstone using nanoindentation, scanning electron microscopy and automated mineralogy. Int. J. Rock Mech. Min. Sci. 125, 104158.

Mo, C.K., Zhao, J.L., Zhang, D.X., 2022. Real-time measurement of mechanical behavior of granite during heating-cooling cycle: a mineralogical perspective. Rock Mech. Rock Eng. 55 (7), 4403–4422.

Nicksiar, M., Martin, C.D., 2012. Evaluation of methods for determining crack initiation in compression tests on low-porosity rocks. Rock Mech. Rock Eng. 45 (4), 607–617.

Pan, S.Y., Gao, M.Y., Shah, K.J., et al., 2019. Establishment of enhanced geothermal energy utilization plans: barriers and strategies. Renew. Energy 132, 19–32.

Peng, J., Rong, G., Cai, M., Zhou, C.B., 2015. A model for characterizing crack closure effect of rocks. Eng. Geol. Ser. 189, 48–57.

Perkins, T.K., Gonzalez, J.A., 1985. The effect of thermoelastic stresses on injection well fracturing. Soc. Petrol. Eng. J. 25 (1), 78–88.

Qin, Y., Tian, H., Xu, N.X., Chen, Y., 2020. Physical and mechanical properties of granite after high-temperature treatment. Rock Mech. Rock Eng. 53 (1), 305–322.

Sha, S., Rong, G., Chen, Z.H., Li, B.W., Zhang, Z.Y., 2020. Experimental evaluation of physical and mechanical properties of geothermal reservoir rock after different cooling treatments. Rock Mech. Rock Eng. 53 (11), 4967–4991.

Vázquez, P., Shushakova, V., Gómez-Heras, M., 2015. Influence of mineralogy on granite decay induced by temperature increase: experimental observations and stress simulation. Eng. Geol. Ser. 189, 58–67.

Wu, X.G., Huang, Z.W., Song, H.Y., et al., 2019a. Variations of physical and mechanical properties of heated granite after rapid cooling with liquid nitrogen. Rock Mech. Rock Eng. 52 (7), 2123–2139.

Wu, X.G., Huang, Z.W., Zhang, S.K., et al., 2019b. Damage analysis of high-temperature rocks subjected to LN_2 thermal shock. Rock Mech. Rock Eng. 52 (8), 2585–2603.

Xie, Z.X., Huang, Z.W., Li, G.S., et al., 2024a. The effect of natural fractures on the failure mechanism of granite: implication for enhanced geothermal systems. Eng. Fract. Mech. 299, 109938.

Xie, Q., Tian, X., Zeng, Y., et al., 2024b. Study on the influence of indentation depths on the fracture characterization and acoustic emission characteristics of minerals in granite using nanoindentation. Constr. Build. Mater. 450, 138516.

Yang, S.Q., Ranjith, P.G., Jing, H.W., Tian, W.L., Ju, Y., 2017. An experimental investigation on thermal damage and failure mechanical behavior of granite after exposure to different high temperature treatments. Geothermics 65, 180–197.

Yin, Q., Wu, J.Y., Jiang, Z., et al., 2022. Investigating the effect of water quenching cycles on mechanical behaviors for granites after conventional triaxial compression. Geomech. Geophys. Geo. 8 (2), 77.

Yin, W.T., Feng, Z.J., Zhao, Y.S., 2021. Effect of grain size on the mechanical behaviour of granite under high temperature and triaxial stresses. Rock Mech. Rock Eng. 54 (2), 745–758.

Zhang, S.S., Zhang, L., Tian, C.C., Cai, J.S., Tang, B.C., 2019a. Occurrence geological characteristics and development potential of hot dry rocks in Qinghai Gonghe Basin. Int. J. GeoMech. 25 (4), 501–508.

Zhang, C., Jiang, G.Z., Jia, X.F., et al., 2019b. Parametric study of the production performance of an enhanced geothermal system: a case study at the Qiabuqia geothermal area, northeast Tibetan plateau. Renew. Energy 132, 959–978.

Zhao, Z.H., 2016. Thermal influence on mechanical properties of granite: a microcracking perspective. Rock Mech. Rock Eng. 49, 747–762.

Minghui Li is a Professor at College of Civil and Transportation Engineering, Shenzhen University, China. He obtained his Ph.D. in Mining Engineering from Chongqing University in 2016. He serves as the vice director of the Guangdong Provincial Key Laboratory of Deep Earth Science and Geothermal Energy Exploitation and Utilization. His main research interests include rock deformation and fracture mechanisms, fluid seepage mechanisms under complex stress conditions, and the prevention and control of dynamic disasters in deep engineering. He has led projects such as the National Key Research and Development Program (Youth Scientist Project), the National Natural Science Foundation of China, and a sub-project of the National Deep Earth Major Program. He has published over 100 academic papers with an H-index of 34 (WOS).